POST-PEROVSKITE $MGSIO_3$ INVESTIGATED BY FIRST PRINCIPLES

TAKU TSUCHIYA[1], JUN TSUCHIYA[1], AND RENATA M. WENTZCOVITCH
Chemical Engineering and Materials Science, Minnesota Supercomputing Institute for Digital Simulation and Advanced Computation, University of Minnesota, Minneapolis, MN 55455, USA

[1]Now at Geodynamics Research Center, Ehime University, Matsuyama 790-0903, Japan

A high-pressure phase transition in iron free $MgSiO_3$ perovskite, the most abundant Earth forming mineral phase, was discovered and reported in 2003-2004. Here, we summarize our theoretical and computational studies on this phase transition and on the physical properties of the newly found post-perovskite phase. The theoretical approach is based on density functional theory and on the plane-wave pseudopotetial method. We focus here on structural, elastic, vibrational, and thermodynamic properties of the post-perovskite phase. The predicted Clapeyron slope of this transition and several elastic properties of the high-pressure phase strongly suggest that this new phase is an important candidate for a primary constituent in D".

1. Introduction

Phase transitions of Earth forming materials dominate the structure and dynamics of the Earth (e.g., Helffrich and Wood, 2001). Major changes in seismic velocity traveling through the Earth's mantle can be attributed to phase transitions of the constituent minerals. Exploration and investigation of high-pressure phase change in the predominant MgO-FeO-SiO_2 system have therefore been one of the central problems in the Earth science for a long time. The high-pressure *Pbnm*-perovskite polymorph of $MgSiO_3$ (hereafter pv) (Liu, 1974) is believed to be the most abundant mineral in the Earth's lower mantle (Knittle and Jeanloz, 1987). The possibility of a phase transition in this polymorph has been controversial for several years. Reports of its dissociation into SiO_2 and MgO at 70-80 GPa and 3000 K (Meade et al., 1995; Saxena et al., 1996), or of a possibly subtle phase change above 83 GPa and 1700 K (Shim et al., 2001), or of no phase transition at all (Fiquet et al., 2000) up to 94 GPa and 2500 K, have appeared in the literature. Although the pressure-temperature (*P*-*T*) conditions in these experiments were quite high, none of them had achieved the thermodynamics state expected in the D" region. Recently, a post-perovskite (ppv) transition in $MgSiO_3$ was found by in situ X-ray diffraction in a diamond anvil cell at ~2500 K and ~125 GPa (Murakami et al., 2004). This *P*-*T* condition is similar to that expected in the D" layer near the core-mantle boundary (CMB). The ppv structure was independently identified by first principles variable cell shape calculations and its thermodynamic properties were obtained by means of quasiharmonic free energy calculations (Tsuchiya et al., 2004b; Tsuchiya et al., 2005a). The predicted Clapeyron slope of the ppv transition was ~7.5 ±0.5 MPa/K, which is surprisingly close to that claimed to be necessary for a solid-solid transition to account for the D" discontinuity (Sidorin et al., 1999). These

results also supported by another study (Oganov and Ono, 2004) suggest that the ppv phase might be the most abundant mineral in the D" region. The ppv phase transition with this large positive Clapeyron slope could enhance mantle convection (Nakagawa and Tackley, 2004) and substantially affect generation of superplume (Matyska and Yuen, 2005). Therefore, understanding of the ppv transition and the properties of the ppv phase is essential for understanding the deep lower mantle, particularly of the D" region (Lay and Helmberger, 1983; Lay et al., 1998; Wysession et al., 1998; Wysession et al., 1999). Knowledge of seismic velocities and elastic anisotropy at relevant pressures is also important for understanding the characteristic velocity discontinuities and anisotropy observed in D". Here we summarize our first principles computational results obtained so far, in particular, structural, thermodynamic, and elastic properties of ppv $MgSiO_3$.

2. Theoretical methods

Within this theoretical framework a solid is viewed as an interacting many-particle system of nuclei and electrons. To solve the many-particle problem exactly is impossible. Some simplifications and approximations are needed to obtain solutions with reasonable computational efficiency. First-principles approaches are those that solve the fundamental equations of quantum mechanics with a bare minimum of approximations. Here we briefly describe the essence of a method based on the density functional theory, which has found wider application in the study of the Earth's interior.

Density functional theory (DFT), originally developed by Hohenberg and Kohn (1964) and Kohn and Sham (1964), is, in principle, an exact theory of the ground state and allows us to reduce the interacting many-electron problem to a single-electron problem (the nuclei being treated as an adiabatic background). Within this theory the charge density is the central quantity and the ground state total energy of a system is a unique functional of the charge density $n(\mathbf{r})$:

$$E[n(\mathbf{r})] = F[n(\mathbf{r})] + \int V_{\text{ion}}(\mathbf{r}) n(\mathbf{r})\, d\mathbf{r}\,. \qquad (1)$$

Here functional $F[n]$ contains the electronic kinetic energy and all the electron-electron interactions and is independent of the external potential, which is usually the Coulomb potential V_{ion} due to ions (or nuclei) plus possibly other external fields. A key to the application of DFT in handling the interacting electron gas was given by Kohn and Sham (1964) by splitting up the kinetic energy of a system of interacting electrons into the kinetic energy of noninteracting electrons plus some remainder which can be conveniently incorporated into the exchange-correlation energy, whose explicit form is not known and contains all the many-body effects in an interacting system.

Using the variational principle implied by properties of the energy functional, one can derive the effective single-electron Schrödinger equation, well known as the Kohn-Sham (KS) equation. The KS equation constitutes a self-consistent field problem; that is, the self-consistent solutions (electronic wave functions and eigenvalues) can be obtained by iteratively solving the KS equation. Then the total energy E can be computed. To solve the Kohn-Sham equations exactly requires knowledge of the exact exchange-correlation functional. For the simple case of the uniform electron gas, the explicit expression for the exchange component is known from the Hartree-Fock theory,

but the correlation component is known only numerically from quantum Monte-Carlo calculations (Ceperley and Alder, 1980; Perdew and Zunger, 1981). The charge density in real materials is not uniform, so the exchange-correlation functional cannot be calculated precisely. The local density approximation (LDA) (Kohn and Sham, 1964) replaces the exchange-correlation potential at each point **r** by that of a homogeneous electron gas with a density equal to the local density at point **r**.

The LDA works remarkably well for a wide variety of materials, especially for silicates; the equation of state, elastic constants, and other properties often agree with experiment to within a few percent. Agreement with laboratory measurements is not perfect, however, and some systematic discrepancies are apparent for some materials. Attempts to improve LDA through consideration of non-local corrections have met with some success. The generalized gradient approximation (GGA) (Perdew et al., 1996) is a marked improvement over LDA for certain cases of transition metals (Bagno et al., 1989; Stixrude et al., 1994) and hydrogen bonded system (Hamann, 1997). There is some evidence that GGA improves the energetics of silicates and oxides but structures tend to be underbound: The volume calculated with GGA tends to be larger than that measured experimentally (Hamann, 1996; Demuth et al., 1999; Tsuchiya and Kawamura, 2001). For $MgSiO_3$ LDA and GGA calculations including zero-point motion tend to overestimate equilibrium volumes and underestimate bulk moduli, with deviations being much smaller with the former (see Wentzcovitch et al., 2004a and references therein).

There are various self-consistent methods for solving the Kohn-Sham equation differing from each other mainly in two aspects: (1) inclusion of all electrons in the calculations or use of pseudopotentials, and (2) details of the basis functions used to expand the electronic wave functions. In all “all-electron” full potential approaches, no approximations are made to the shape of the charge density or the potential and they are generally accepted to be highly accurate and suitable to all types of crystals irrespective of their bonding nature. However, representation of the rapidly varying core states makes all-electron calculations relatively intensive computationally. The idea behind the of plane-wave-pseudopotential-method (PWPP), by which all the results shown in this article were obtained, is that the precise representation of the core states is not essential because they do not participate in bonding. The strong potential due to the nucleus and core electrons is replaced by a soft, more slowly varying potential with the same scattering properties (pseudopotential). This approach speeds up calculations substantially because (1) only valence electrons are treated explicitly and (2) the pseudocharge density and potential vary much more slowly in space. The latter feature is particularly allows one to use plane waves as the basis functions to represent the electronic wave function at each wave vector **k**. Evaluation of total energies, forces, and stresses with the plane wave basis set is particularly efficient (Nielsen and Martin, 1985). Construction of the pseudopotential is a non-unique process, but differences between different pseudopotentials (Hamann et al., 1979; Vanderbilt, 1990; Troullier and Martins, 1991), and between PWPP and all electron calculations, are often smaller than the uncertainties due to approximations to the exchange-correlation potential.

Properties of materials in their ground state are obtained through variational calculations that minimize the total energy of the system with respect to all degrees of freedom, electronic and ionic. The charge density is the quantity that must be varied for

minimization with respect to electronic degrees of freedom, and ionic positions and lattice parameters are the ionic the corresponding ones. One can then obtain various physical properties starting from the stable structure; elastic constant tensor, thermodynamic property and so on.

The plane wave pseudopotential approach, which combines accuracy, computational efficiency, and formal simplicity, has been developed to the point of being used in the context of molecular dynamics (MD) simulations. This facilitated the implementation of a variable-cell-shape-MD (VCSMD) formalism (Wentzcovitch et al., 1993). This type of simulation is particularly useful in high-pressure studies. Its flexible periodic boundary conditions can capture dynamically even structural phase transitions under pressure and is useful in investigations of complex low-symmetry structures typical of the Earth forming minerals.

In contrast, the central quantity in lattice-dynamics calculations is the dynamical matrix

$$D^{\alpha\beta}_{\kappa\kappa'}(\mathbf{q}) = \frac{1}{\sqrt{m_\kappa m_{\kappa'}}} \sum_l \Phi^{\alpha\beta}_{\kappa\kappa'}(0l) \exp[-i\mathbf{q}\cdot(x_0 - x_l)]. \tag{2}$$

Here the interatomic force constants $\Phi^{\alpha\beta}_{\kappa\kappa'}(0l)$ include ionic and electronic contributions, the former being calculated from Evald sums and the latter being expressed as

$$\Phi^{\alpha\beta}_{\kappa\kappa'}(0l) = \int \left[\frac{\partial\rho(\mathbf{r})}{\partial u^\alpha_\kappa(0)} \frac{\partial V_{\text{ion}}(\mathbf{r})}{\partial u^\beta_{\kappa'}(l)} + \rho(\mathbf{r}) \frac{\partial^2 V_{\text{ion}}(\mathbf{r})}{\partial u^\alpha_\kappa(0) \partial u^\beta_{\kappa'}(l)} \right] d^3r \,, \tag{3}$$

where $\rho(\mathbf{r})$ is the electron density, $V_{\text{ion}}(\mathbf{r})$ is the ionic potential, and $\partial\rho(\mathbf{r})/\partial u^\alpha_\kappa(0)$ represents the density response of the system to a displacement of the κ atom in the reference cell (l = 0) along the α direction. This linear electron density response can be calculated self-consistently using density functional perturbation theory (Baroni et al., 2001). At a given pressure (or volume), first the structure is fully optimized. Then the dynamical matrices are computed, and are used for interpolation to obtain bulk phonon dispersions. These methods have been successfully applied to MgO, SiO_2 polymorphs, $MgSiO_3$ ilmenite and perovskite (Karki et al., 2000a; Karki et al., 2000b; Wentzcovitch et al., 2004a; Tsuchiya et al., 2004a).

In polar semiconductors and insulators, phonons are coupled to macroscopic electric field in the long-wavelength limit. The non-analytical contribution of the macroscopic electric field to the force constant tensor is given by

$$\frac{4\pi e^2}{V} \frac{(\mathbf{q}\cdot\mathbf{Z}^*_\kappa)_\alpha (\mathbf{q}\cdot\mathbf{Z}^*_{\kappa'})_\beta}{\mathbf{q}\cdot\boldsymbol{\varepsilon}_\infty\cdot\mathbf{q}}, \tag{4}$$

where the tensors $\mathbf{Z}^*$ and $\boldsymbol{\varepsilon}_\infty$ are, the Born effective charges and macroscopic high-frequency static dielectric constant which are calculated self-consistently, respectively (Baroni et al., 2001).

When the volume dependence of the thermal energy is represented within the quasiharmonic approximation (QHA) (Wallace, 1972), the internal energy and Helmholtz free energy take the following forms,

$$U(V,T) = U_0(V) + \frac{1}{2}\sum_{\mathbf{q},i} h\omega_i(\mathbf{q},V) + \sum_{\mathbf{q},i} \frac{1}{e^{h\omega_i(\mathbf{q},V)/k_BT} - 1} \tag{5}$$

and

$$F(V,T) = U_0(V) + \frac{1}{2}\sum_{\mathbf{q},i} h\omega_i(\mathbf{q},V) + k_B T \sum_{\mathbf{q},i} \ln\left[1 - e^{-h\omega_i(\mathbf{q},V)/k_B T}\right], \quad (6)$$

where the first, second, and third terms are the static lattice, zero-point and thermal contributions, respectively. This approximation neglects the temperature dependence of phonon frequencies at the constant volume condition. Other thermodynamic quantities (pressure P, vibrational entropy S, specific heats C_P, C_V , thermal expansivity α, bulk moduli B_T, B_S, Grüneisen parameter, etc. are derived from their thermodynamic or statistical mechanical definitions. At zero pressure, the predicted temperature dependence of α appears to be significantly biased by the QHA leading to unusually large values at very high temperatures. As pressure rises, a rapidly decreases at each temperature, and also the effects of temperature are increasingly suppressed, thus converging to a nearly constant value in the limit of high pressure and high temperature.

The determination of the elastic constants proceeds: 1) at a given pressure (or volume) the crystal structure is first fully optimized, 2) the lattice is slightly deformed by applying a small strain. The stress in the strained configuration is calculated, and the values of the elastic constants follow from the linear stress-strain relation

$$\sigma_{ij} = c_{ijkl}\varepsilon_{kl} . \quad (7)$$

In elastic constant calculations, 1) the ionic positions need to be reoptimized in the strained lattice in order to incorporate any couplings between strains and vibrational modes in the crystal (Nastar and Willaime, 1995) and 2) the elastic constants need to be computed in the appropriate limit of zero strain. At finite strain, higher-order terms in the stress-strain relationship become important. To calculate the elastic constants in the linear regime, strains of different magnitude or sign are applied, and the zero-strain limit is determined by extrapolation or interpolation. This linear regime is the most relevant in geophysics.

3. Post-perovskite crystal structure

The search for the ppv structure was guided by two general principles: (a) polyhedron types and interconnections that would be reasonable at ultrahigh pressures; and (b) extrapolation of the compressive mechanism of the *Pbnm*-pv structure. Edge-sharing rutile-like columns form a more compact octahedral arrangement, but the stoichiometry requires these columns to be connected by the octahedral apices. This produces the SiO_3 layers. These layers should then be intercalated by magnesium ions with the highest possible coordination (Fig. 1). These criteria produce a family of structures. All attempted structures were fully optimized above 120 GPa using variable cell shape damped molecular dynamics, and their enthalpies were then compared with *Pbnm*-pv's. The structure (last figure in Fig. 1) is the only one we found with lower enthalpy than pv in static LDA and/or GGA calculations. This is the structure of $CaIrO_3$ (Hyde and Andersson, 1989), the same one found experimentally (Murakami et al., 2004). This structure is base-centered orthorhombic (BCO) with space group *Cmcm*. Magnesium ions are located in approximately eightfold-coordinated sites, at the center of irregular hendecahedra. It has four formulae unit per conventional cell (Z_c = 4) like the *Pbnm* pv structure, two unit per primitive cell (monoclinic, Z_p = 2), but it is very anisotropic.

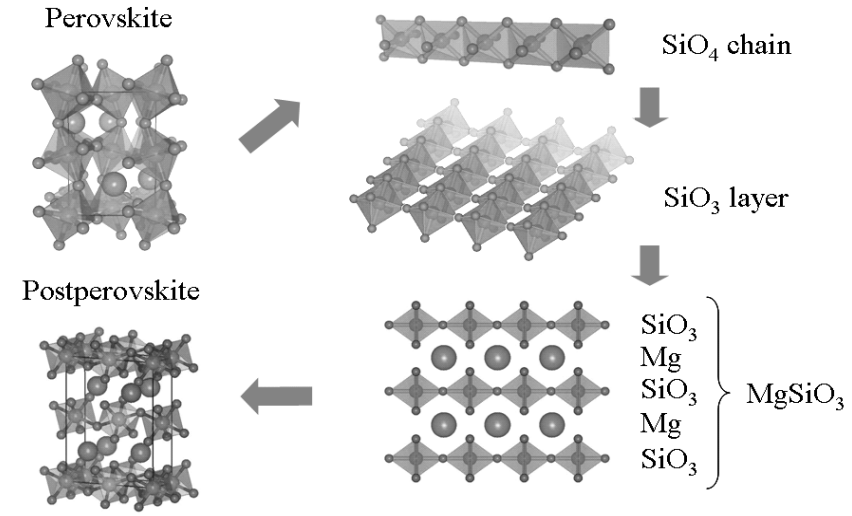

Fig.1. Strategy of the structural search for ppv. Small and large spheres are oxygen and magnesium ion and octahedron corresponds with SiO_6 unit. Detailed calculated crystallographic data of ppv, along with those of pv, are given in Tsuchiya et al. (2004b).

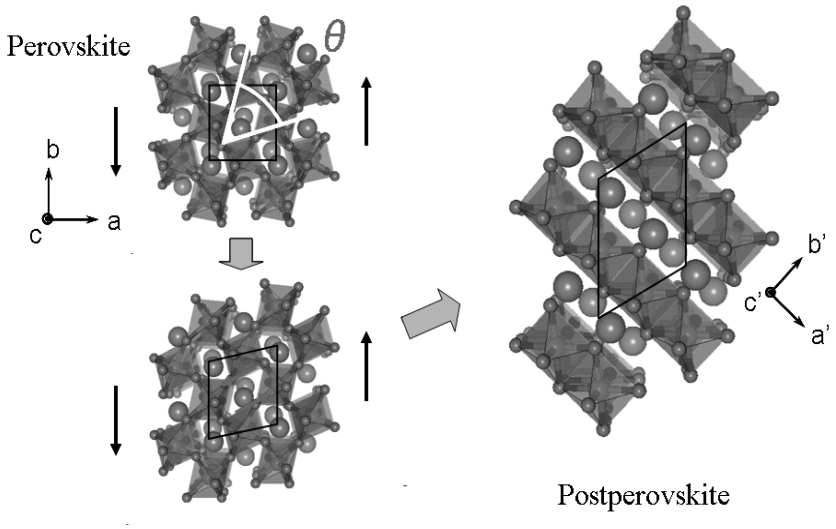

Fig.2. Structural relation between pv and ppv under shear deformation of ε_6. θ indicates the octahedra tilting angle which decreases the fastest with hydrostatic compression of pv.

Static isotropic compression using LDA revealed a transition pressure of 98 ± 3 GPa (109 ± 4 GPa using the GGA).

The relationship between this *Cmcm* and the *Pbnm* structures (Fig. 2) can be understood on the basis of the extrapolated compressive behavior of $MgSiO_3$-pv (Wentzcovitch et al., 1995). The angles between the octahedral edges bisected by the (110) plane in the *Pbnm* structure decrease faster than other similar angles. The *Cmcm* structure can be produced by forcing these angles to close faster under strain ε_6. Fig. 2 shows structures that result by applying strains ε_6 in the *Pbnm*-pv first equilibrated at 120 GPa. For sufficiently large strains, these angles vanish and form edge-sharing rutile columns when one of the oxygens in each pair of edges defining these angles is removed. This process forces layer formation. In the third direction, perpendicular to the columns and to the layers, octahedra remain connected at the apices. According to this transition mechanism, the $[100]_{ppv}$, $[010]_{ppv}$, and $[001]_{ppv}$ directions in the *Cmcm* structure correspond to the $[110]_{pv}$, $[1\bar{1}0]_{pv}$, and $[001]_{pv}$ in the *Pbnm* structure, respectively. Structural parameters obtained in static LDA calculations at 120 GPa are given in elsewhere (Tsuchiya et al., 2004b).

Fig. 3 shows compression curves of pv and ppv at various temperatures. In the relevant pressure range, ppv is always denser than pv. At the transition pressure, which of course depends on temperature, volume decreases approximately by 1.5%. Ppv compresses very anisotropically. The *b* axis perpendicular to the SiO_3 layers compresses faster than the others. The inset shows the pressure dependence of the *b*/*a* and *c*/*a* ratios in this phase as obtained from static calculations. As expected, the structure is more compressible along [010]. Right figures of Fig. 3 are the charge

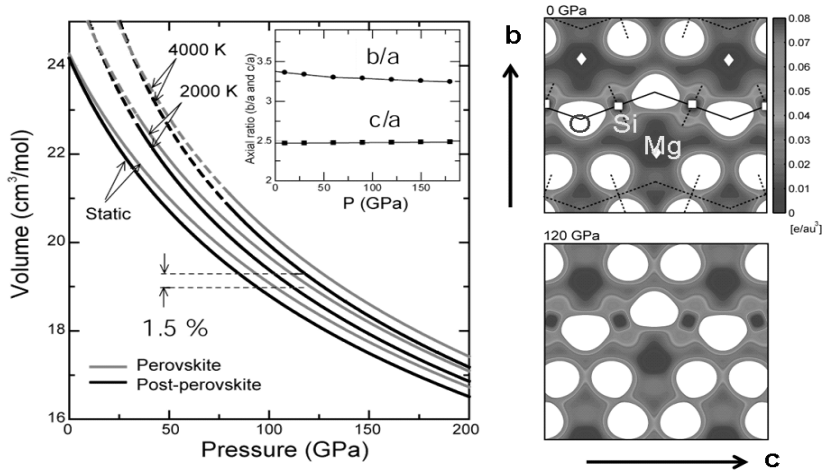

Fig.3. *PT* compression behavior of pv and ppv. Isothermal compression curves are shown in left panel together with change in axial ratios in the inset. Volume decrease across the transition is ~1.5%. Pseudocharge densities across (100) at 0 and 120 GPa are also shown in the right side.

density in the (100) plane that cut across the SiO_3 layers. Vertical is the *b* direction. Magnesium (diamonds) is almost completely ionized. Strong Si (square)-O (center of white hole) bonds are within the layers. Mg-O bonds connecting the layers are ionic and weak. Therefore the structure is more compressive along *b*.

4. Vibrational and thermodynamic properties

4.1. PHONONS

Vibrational and thermodynamic properties are helpful for better understanding the basic properties of the ppv phase and to further explore the importance of this phase as a D" constituent. Comparison between the thermal expansivity, specific heat, and entropy of pv and of the ppv phase is essential to clarify the effect of this transformation on mantle dynamics also. However, experimental measurements of these properties under lower mantle conditions are not yet possible. Here we use the QHA combined with first principles calculations of the vibrational density of states to compute the free energy of $MgSiO_3$ ppv and derive several thermodynamic properties of interest up to 180 GPa. We then compare with the same properties previously calculated in the pv phase (Karki et al., 2000a; Karki et al., 2001). There are 30 vibrational modes at any point in the BZ because $Z_p = 2$.

The predicted dispersion curves along several symmetry directions and vibrational density of states (VDoS) at 0 and 120 GPa are shown in Fig. 4a. Though 0 GPa is obviously outside of its stability fields, these results are informative and indicative of

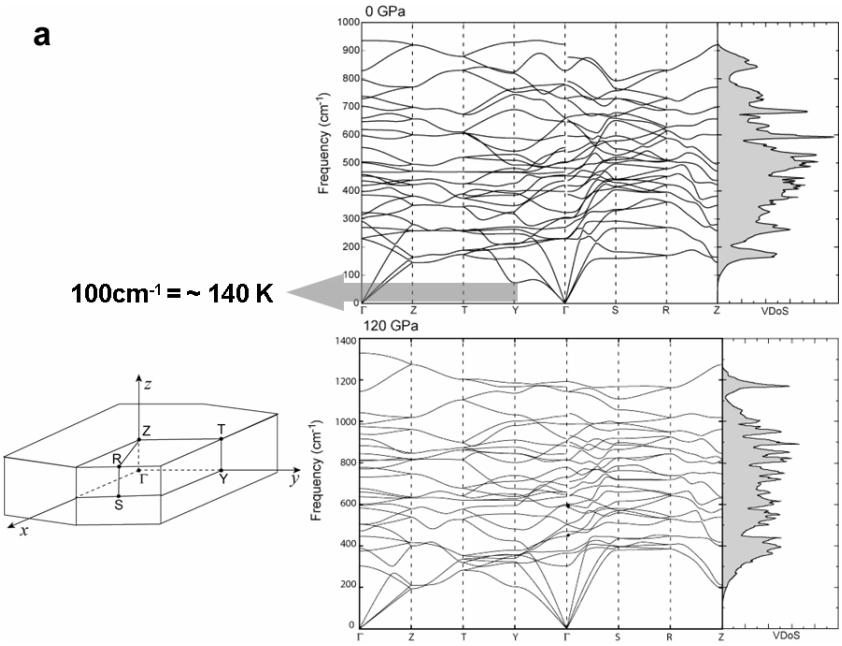

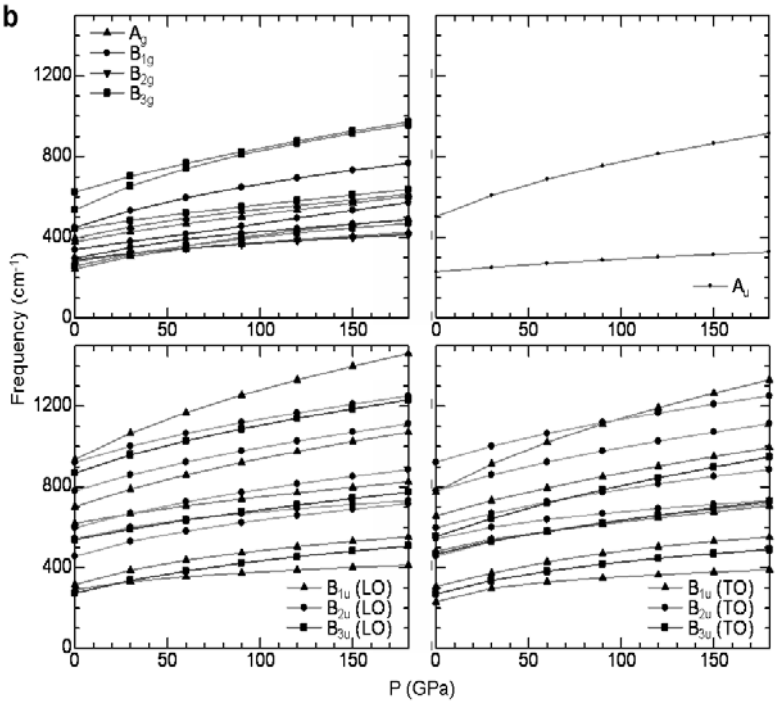

Fig.4. Vibrational frequencies in ppv. (a) Phonon dispersion relation at 0 (up) and 120 GPa (down) together with the *Cmcm* Brillouin zone. (b) Pressure dependence of zone center optic phonons.

the mechanical/vibrational stability of this phase. Under decompression the lowest acoustic branch starts drooping down around the Y point of the BZ (Fig. 4a). This behavior is associated with the easier elongation of *b* axis under decompression. Zone center optic phonon frequencies are shown in Fig. 4b as a function of pressure. They are grouped with respect to symmetry which has been determined by the factor group analysis. No phonon instability is found in the entire range of pressure even at 0 GPa. The diagonal components of the dielectric tensor are 3.53, 3.22, and 3.24 at zero pressure, and 3.27, 3.04, and 3.03 at 120 GPa. Born effective charges for Mg are close to the formal ionic charges of magnitudes equal to 2 and are weakly anisotropic: Z^* [Mg] = (2.00, 2.36, 2.13) at zero pressure and Z^* [Mg] = (1.85, 2.14, 2.00) at 120 GPa. However, those for Si and O are very anisotropic: Z^* [Si] =(3.98, 2.93, 3.60), Z^* [O(1)] = (−1.45, −1.55, −2.50), and Z^* [O(2)] = (−2.26, −1.87, −1.62) at zero pressure, and Z^* [Si] = (3.79, 2.99, 3.51), Z^* [O(1)] = (−1.49, −1.55, −2.34), and Z^* [O(2)] = (−2.08, −1.79, −1.59) at 120 GPa.

4.2. THERMODYNAMIC PROPERTIES

We then proceeded with calculations of phonon dispersions and vibrational densities of states (VDOS) (see Fig. 4a) to obtain Gibbs free energies within the QHA. At 300 K, the zero-pressure bulk modulus, B_0 = 216 GPa, is substantially smaller than pv's, 246 GPa. However, the pressure derivative of the bulk modulus, B_0' = 4.4, is distinctly larger than pv's, 4.0, where these EoS parameters were determined using the fourth-order finite strain equation. The zero-pressure Grüneisen parameter, ~1.7, and the Debye temperature, Θ_D ~1100 K, are fairly comparable to those of pv. Comparison between the volumes of both phases at the same *P*-*T* conditions indicates that the ppv phase is always denser than pv (see Fig. 3).

The coefficient of thermal expansion α is determined from the temperature dependence of volume at each pressure (Fig. 5). At zero pressure, the predicted temperature dependence of α appears to be significantly biased by the QHA leading to unusually large values at very high temperatures. As pressure rises, α rapidly decreases at each temperature, and also the effects of temperature are increasingly suppressed, thus converging to a nearly constant value in the limit of high pressure and high temperature. At lower pressure, the thermal expansion coefficient of pv is quite smaller than ppv's. The difference between pv and ppv decreases with increasing pressure. Above 100 GPa, α of pv and of ppv are nearly the same.

Because of the expected high temperatures in the mantle, the validity of QHA is often questioned. However, it should be valid up to some temperature between the Θ_D and the melting temperature (T_M), the latter being considerably higher than expected mantle temperatures. The calculations of thermal properties of MgO (Karki et al., 2000b) and $MgSiO_3$ (Wentzcovitch et al., 2004b) have indicated that the QHA is valid for these phases throughout the lower mantle regime. A posteriori inspection of their thermal expansivities, $\alpha(T)|_P$, offers a criterion for the QHA validity domain. Experimentally $\alpha(T)|_P$, displays linear behavior at high *T*'s but the QHA introduces an unphysical divergence after some inflection point at $T = T_I(P)$. We take $T_I(P)$ as the upper limit for which our results should be considered predictive. This criterion indicates the QHA is valid for pv and ppv within the *P*, *T* regime of the lower mantle, except perhaps at the top of the lower mantle, i.e., at *P* = 23 GPa and *T* = 1900~2000 K. On the basis of this criterion alone, the valid temperature and pressure conditions of the QHA for ppv appears to be similar to that of pv. This criterion appears to be quite strict for the free energies themselves, but perhaps not sufficiently strict for quantities involving temperature derivatives such as the constant volume specific heat, C_V , α, etc. The thermal Grüneisen parameter γ may be particularly sensitive to this approximation since it involves two temperature derivative quantities, α and C_V. Below 30 GPa, ppv's γ increases rapidly, and so does its temperature dependence. This behavior seems anomalous and might be caused by the inadequacy of the QHA for this quantity in this regime.

The specific heat at constant pressure (C_P) calculated from $C_P = C_V (1+\alpha\gamma T)$ and the entropy (*S*) are also shown in Fig. 5, respectively. The difference between C_V of pv and ppv are rather negligible at each pressure. The entropy *S* of ppv is slightly smaller than that of pv at stable pressure conditions giving a Clapeyron slope, $dP_T/dT = \Delta S/\Delta V \approx 7.5$ MPa/K for the ppv transition. The thermodynamic properties reported here are important inputs for geodynamic modeling. Our calculations indicate that the thermal expansivity, specific heat, thermal Grüneisen parameter etc., change very little across

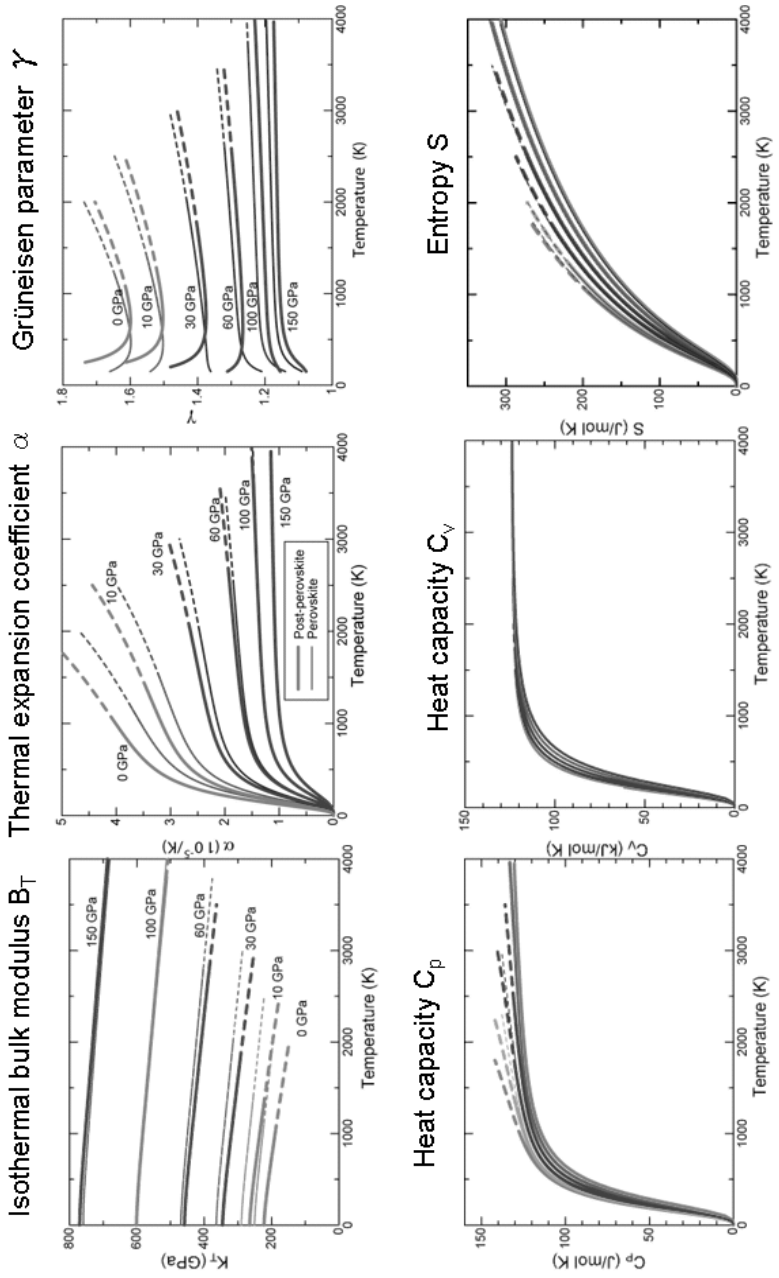

Fig.5 Thermodynamic properties of pv and ppv as a function of temperature. Thick and thin lines are for ppv and pv, respectively. Most of them are indistinguishable at the pressures in ppv stability field.

the ppv transition. Although it has been pointed out that small changes in thermal expansivity lead to significant variations in mantle convection pattern and its time evolution (Ita and King, 1998), it appears that the changes here are quite insignificant for such effects to happen.

4.3. PHASE EQUILIBRIUM

In static calculations, LDA tends to underestimate transition pressures and GGA results are usually in better agreement with experiments. The main source of these deviations is the description of the exchange correlation energy in density functional theory. The inclusion of zero-point motion in the calculation of a phase boundary with positive Clapeyron slope shifts the boundary to higher pressures, ~2 GPa in this case. It is therefore reasonable to anticipate that the true transition pressure falls between the phase boundaries given by LDA and GGA. Direct comparison of the Gibbs free energies of both phases produces the phase boundary. The dP_T/dT at 2500 K is ~7.5 ± 0.3 MPa/K in complete agreement with the value derived from the Clausius-Clapeyron equation.

5. Elasticity

Ppv $CaIrO_3$-type structure is anisotropic. Its elastic properties are also expected to be anisotropic. From the overall behavior of the elastic constants, of which specific values are reported in elsewhere as a function of pressure (Tsuchiya et al., 2004c), it is clear that the structure is quite anisotropic and that anisotropy is strongly pressure dependent. Two particular features can be immediately noticed: 1) c_{22} is considerably smaller than c_{11} and c_{33} at relevant pressures, and 2) c_{66} is quite large compared with c_{55} and c_{44}. The first feature is typical of layered minerals. It shows this structure is more compressive in the direction perpendicular to the layers (layers parallel to (010)). The second feature is very intriguing. It indicates that a lateral shift of layers ((010) planes) parallel to the edge sharing octahedral columns (along [100]) faces the greatest resistance. This is counterintuitive. In a typical layered structure, lateral shear of layers, along any direction, should offer less resistance than the deformation of the layers themselves, here represented by c_{55}. In this structure, the smallest shear elastic constant is c_{44}. It expresses the resistance along [001], i.e., to the lateral shift of layers in the direction perpendicular to the octahedral columns.

The pressure dependence of the isotropic bulk (B) and shear (G) moduli obtained from the Voigt-Ruess-Hill averages (Hill, 1963) are shown in Fig. 6 along with those of the pv structure. It can be seen that B of both phases are very similar throughout most of the pressure range of the lower mantle. The larger B_0 of ppv, 4.3, compensates to produce similar bulk moduli at lower mantle pressures. In contrast, ppv has considerably larger G than pv in the pressure range corresponding to the lower part of the lower mantle (7% larger at 120 GPa) even though ppv's G is smaller than pv's at 0 GPa. This large G is caused by the large c_{66}. The isotropic averaged compressional (P), shear (S) and bulk (Φ) wave velocities are plotted in Fig. 6. At zero pressure, all velocities are smaller than those of pv, while at high pressure, V_P and V_S of ppv are distinctly larger than those of pv. V_Φ is quite comparable. The discontinuity in V_P, V_S

and V_Φ at the static P_T of 100 GPa are 0.5, 1.5 and -0.5%, respectively. The large shear wave velocity of ppv is clearly caused by its large G, despite the larger density of this phase. Negative change in V_Φ is because of density increase and unchanged bulk modulus. The ppv transition should be observed preeminently through S wave anomalies.

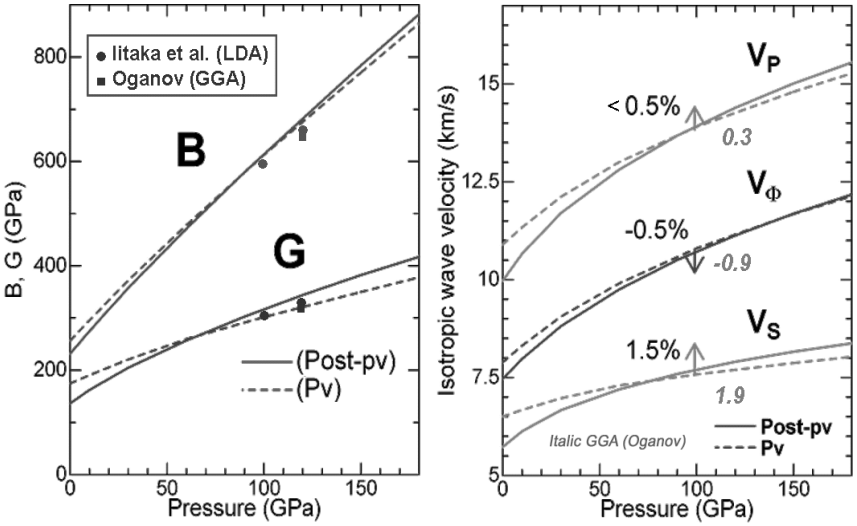

Fig.6. Aggregate elastic moduli and velocities of pv and ppv as a function of pressure. Results are supported well by other works (Litaka et al., 2004; Oganov and Ono, 2004).

The single crystal elastic wave velocities were obtained by solving Cristoffel's equation (Musgrave, 1970). Wave velocities depend on propagation direction and on polarization. For ppv, the difference between V_P and V_S is relatively small compared to the same difference found in pv (Wentzcovitch et al., 1998). This is also caused by the relatively larger G of ppv. Fast and slowest directions change very much with pressure. At 0 GPa V_P is largest and smallest along [100] and [110] respectively. This results from large c_{11} and small c_{66} respectively. At 120 GPa, the slowest direction of the P wave changes to [010], consistent with the small c_{22}. The fastest S waves propagate along [110] and [101], and the slowest along [010] and [001] at 0 GPa. In contrast, at 120 GPa, the fastest directions is along [101] while the slowest are along [100] and [001] (Tsuchiya et al., 2004c).

Azimuthal anisotropy for P (A_P) and S (A_S) waves, defined as $A_P = (V_{Pmax} - V_{Pmin})/V_P \times 100$ and $A_S = (V_{Smax} - V_{Smin})/V_S \times 100$, are plotted in Fig. 7. First, they decrease up to about 100 GPa and then remain almost constant. However, at the stable pressure range of ppv, A_P and A_S are much larger than pv's (A's are more than 50% larger). Single crystal anisotropy gives the upper limit on the realistic anisotropy of aggregates. The magnitude of anisotropy due to the lattice preferred orientation (LPO) in aggregates is, in general, much smaller (by a factor of 2 to 3). Another point relevant for extracting information about mantle flow from seismic observations is the

anisotropy produced by transversely isotropic aggregates. This type of aggregate may be caused by LPO's produced under shear flow and can occur at boundary layers. Shear stresses related with changes in flow direction are expected to be particularly large near the CMB. A transversely isotropic medium with a principal vertical axis is characterized by five elastic moduli determined from single-crystal elastic constants (Wentzcovitch et al., 1998).

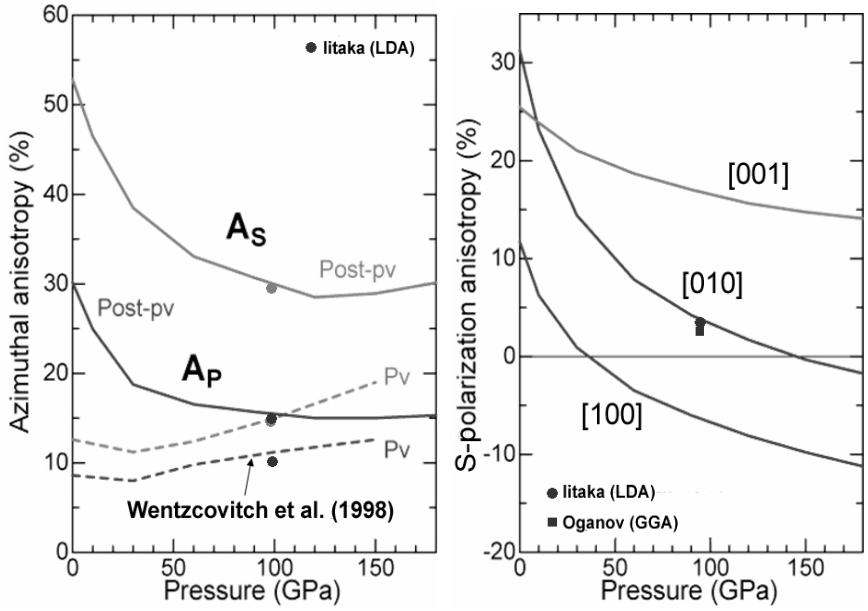

Fig.7. Elastic anisotropies in pv and ppv as a function of pressure.

Transverse anisotropy in V_S is defined as $A_S^T = (V_{SH} - V_{SV})/V_S \times 100$, where V_{SH} (V_{SV}) is horizontally (vertically) polarized V_S propagating horizontally. V_S is the usual isotropic averages. Results are also plotted in Fig. 7 for aggregates with *a*, *b*, and *c* vertical alignment. It can be seen that A_S^T can be positive or negative depending on the crystalline axes orientation. Contrary to expectations for a layered structure with the slip plane parallel to the layers, A_S^T is small in magnitude (~3% at P_T) and becomes negative at high pressure for [010] aligned vertically. This is because of the counterintuitively large c_{66} at high pressures. The positively largest A_S^T (~17% at P_T) is achieved with [001] oriented vertically, i.e., layers oriented vertically. Again this is caused by the large values of c_{66} for vertical orientation of layers. These properties have been supported by other calculations. (Stackhouse et al., 2005)

The phonon dispersions displayed in Fig. 4a reveal an interesting fact about ppv. Although there is an acoustic branch that softens under decompression, at 0 GPa all phonons are still stable. This type of acoustic phonon softening is typical of materials that amorphize under decompression (or compression). The frequencies along this

branch (except around Γ), are in the range of 100 cm^{-1}, i.e., ~140 K. This means that below this typical temperature these phonons are not very populated and therefore ppv may be retrieved metastably at 0 GPa, unless there is some nonobvious elastic instability.

6. Discussion

This transition is important for understanding the state of the deep lower mantle, particularly that of the D" region, the lowest 300 km of the lower mantle (Sidorin et al., 1999; Lay and Helmberger, 1983; Lay et al., 1998; Wysession et al., 1998; Wysession et al., 1999). The D" layer has wide topography (Lay and Helmberger, 1983). Properties of this region vary strongly laterally, including its considerable anisotropy (Wysession et al., 1998). Chemical heterogeneity, partial melting, phase transitions or a combination of all of these have been proposed as possible mineralogical origins of these features and it is likely that all of them indeed play a role in this region. It is also believed that the anisotropy observed in S_H and S_V waves traveling through D" at least in part could be attributed to LPO of strained minerals aggregates (Karato, 1998; McNamara et al., 2002). In particular, it has been argued on the basis of seismic and geodynamic considerations that a solid-solid phase change with a Clapeyron slope of ~6 MPa/K (Sidorin et al., 1999) could cause the observed topography. Our Clapeyron slope of 7.5 ± 0.3 MPa/K is quite close to this value. The major effects of a ppv transition on the dynamics in the lowermost mantle have already been investigated and reported (Nakagawa and Tackley, 2004). This exothermic transition with a large and positive Clapeyron slope enhances mantle convection and accelerates heat release from the core. This results in raising the overall mantle geotherm by ~200 K and also helps to produce small unstable plumes. Large thermal conductivity possibly associated with radiative thermal conduction would be necessary to stabilize superplumes (Matyska and Yuen, 2005). If geotherm is sufficiently high (T > 4000 ~ 4500 at 135 GPa), the ppv transition pressure shifts into the outer core condition. No ppv is therefore expected in the mantle at the stage of hot early Earth. When the ppv transition pressure fell into the mantle pressures and ppv appeared in the mantle along with cooling of the Earth, mantle and core dynamics would have begun to be activated. Geophysical importance of advent of ppv in the history of Earth's evolution is now being investigated (Maruyama, 2005).

Determination of the rheological change across the transformation is now the key issue for assessing the effects of such transformation more realistically. Obviously, effects of minor elements (Al, Fe) partitioning on all properties across the transition also must be considered. This fact might be of minor significance considering that the D" region is a thermochemical boundary layer with strong heterogeneities. The presence of alloying elements, such as aluminum and iron, is likely to affect the transition pressure and the Clapeyron slope, particularly if minor element partitioning between $MgSiO_3$ and other coexisting phases is affected. For instance, silicon and magnesium polyhedral volumes increase and decrease, respectively, across the transformation (Tsuchiya et al., 2004b). This might affect element partitioning. It was reported that iron-bearing pv would transform at lower pressures (Mao et al., 2004). However, the relationship between high- to low-spin transition in iron (Badro et al.,

2003; Badro et al., 2004) and the ppv transition, proposed to occur simultaneously at least in part, is still highly unclear. In contrast, recent results suggest that the Al incorporation does not affect the transition pressure significantly (Murakami et al., 2005; Ono et al., 2005b; Tsuchiya et al., 2005b). The structural relationship between the *Pbnm* and the *Cmcm* phases found here suggests that also shear stresses are likely to affect the transition pressure (in both directions). Shear stresses, although very small compared to those in our investigation, are expected to occur particularly near the CMB. Also, the possibility of an intervening pv phase with different symmetry (Shim et al., 2001) could increase the ppv transition pressure, though this observation itself seems to be interpreted by other cause than pv modification (Ono et al., 2005a).

Our best estimate of the transition temperature in pure $MgSiO_3$-pv through the pressure range of 125-133 GPa is 2750-3800 ± 250 K (Tsuchiya et al., 2004b). These temperatures are consistent with the existence of a ppv transition before the core-mantle boundary where temperatures can reach ~4100 K (Williams and Jeanloz, 1990; Boehler, 1993) and point to the possibility of 1000 K lateral temperature variations in this region. However, D" is very likely a thermo-chemical boundary layer (Lay et al., 2005). Therefore the effect of composition and stress state on this transition still must be investigated before an attempt is made to relate the D" topography and lateral temperature variations through the ppv transition.

Although the elastic wave properties shown here are static 0 K results and high temperature results are necessary before a more reliable analysis of the importance of ppv to D" can be attempted, these results give the first glimpses on the elastic properties of the newly found phase. First, the stability field of ppv appears to correspond well with that expected in the D" layer. We see here that, at the transition point, the discontinuity in V_S should be considerably larger than in V_P. This is consistent with reports that the velocity anomaly at the D" discontinuity is more preeminent in V_S than in V_P (Wysession et al., 1998). In contrast, the discontinuity in V_Φ is negative. This indicates that the ppv transition can cause the anticorrelation between S and bulk velocities observed in tomographic images at the bottom of mantle (Masters et al., 2000), which is one of the most enigmatic properties observed in this region. The D" region is also known to be much more anisotropic than the lower mantle (Lay et al., 1998) and the anisotropy style, i.e., $V_{SH} > V_{SV}$ or vice-versa, varies considerably from place to place (Pulliam and Sen, 1998).

LPO in this structure can be a source of anisotropy in this region. Here we show that ppv's static azimuthal anisotropy (Fig. 7) is much larger (by 50%) than pv's. This is primarily caused by the small and very large values of c_{22} and c_{66}, respectively. The contrast between pv's and ppv's anisotropies could, in principle, produce seismically detectable anisotropy changes across the transition in addition to velocity discontinuities. We also see that the transverse shear anisotropy is very large in magnitude for more than one LPO, in addition to changing sign. Although real fabrics with LPO formed under shear stresses should have some azimuthal anisotropy in the shear plane and should not be completely transversely isotropic, and a better understanding of the rheological properties of ppv is necessary before anything can be stated with more confidence, here we can anticipate from the property of the transversely isotropic medium that LPO's produced by vertical or horizontal flows in D" could produce quite distinct shear wave splittings. This appears to be consistent

with the documented lateral variation of anisotropy in D" (Lay et al., 1998). The anisotropy style observed underneath the circum-Pacific, i.e., $V_{SH} > V_{SV}$, could be produced by vertical alignments mainly of [001], but perhaps also of [010] (Fig. 7). The former is however much more significant than the latter, contrary to expectations for this layered structure. These elastic properties of ppv indicate that at high pressures the usual notion of a layered structure is not simply applicable to this phase.

Magnesiowüstite (Mg,Fe)O, the expected secondary abundant phase, is also very anisotropic, and another likely candidate for the origin of seismic anisotropy in the D" (Karki et al., 1999; Yamazaki and Karato, 2002). Mw aggregates with [100] oriented vertically could produce much larger (>20%) positive S wave splitting at the D" condition. (100) is the expected natural slip plane in this mineral and, thus, even in smaller amount, mw cold be the main source of LPO derived anisotropy in D". In this case, significant change in the deformation mechanism of mw, from dislocation to diffusion creep, must accompany the ppv transition. However, the elasticity of mw including low-spin to high-spin transition in iron is still unknown. The proper description of electronic transitions such as this one, is a major challenge in theoretical mineral physics today.

In summary, we have shown that $MgSiO_3$-ppv is a highly anisotropic phase. Aggregates of this phase with mw could be a source of LPW derived anisotropy in D". For more complete understanding of the origin of D" anisotropy, detailed information on elasticity and plasticity of these two phases aggregates (ppv+mw) at high temperatures, including the effects of Fe, still need to be considered. To this list one should add $CaSiO_3$-pv. Despite its small abundance, its elasticity is quite "suspicious" because of the large number of nearly stable pv-distortions in this mineral. This indicates this mineral is stabilized by anharmonic fluctuations and is constantly on the verge of stress induced structural transitions (Caracas et al., 2005). After all these factors have been properly addressed the importance of chemical stratification and partial melting in generating the observed anisotropy style where the ppv transtition is most likely to occur, $V_{SH} > V_{SV}$ (Kendall and Silver, 1996), can be more fully appreciated.

7. Conclusion

A new polymorph of $MgSiO_3$ with the $CaIrO_3$ structure and more stable than the *Pbnm*-pv phase has been identified by first principles computations. The $CaIrO_3$ structure is shown to be related with the *Pbnm*-pv structure through a shear strain σ_6. This very simple structural relationship suggests that the ppv phase transition pressure might be affected by shear stresses. Quasiharmonic high-temperature calculations of the thermodynamic phase boundary gives a Clapeyron slope of ~7.5 MPa/K at ~2750 K and ~125 GPa. These *P*-*T* conditions are close to those anticipated in the D" region and this Clapeyron slope is close to that anticipated if the D" topography were related to a solid-solid transformation. Thermodynamic properties of ppv are very similar to those of pv at relevant pressures. Some of them are indistinguishable. The anticorrelated anomaly in V_S and V_Φ and the positive S wave splitting have been known as particular observables in the deep mantle which have never been explained well. The ppv transition can produce this type of anticorrelation. A transversely isotropic medium of

ppv with [001] oriented vertically can produce the very large positive S wave splitting. These results strongly suggest that the ppv transition might be associated with the D" discontinuity and that this polymorph might be the most abundant phase in D".

8. References

Badro, J., G. Fiquet, F. Guyot, J.-P. Rueff, V.V. Struzhkin, G. Vanko, G. Monaco (2003) Iron partitioning in Earth's mantle: Toward a deep lower mantle discontinuity, *Science*, **300**, 789-791.

Badro, J., J.-P. Rueff, G. Vanko, G. Monaco, G. Fiquet, F. Guyot (2004) Electronic transitions in perovskite: possible nonconvecting layers in the lower mantle, *Science*, **305**, 383-386.

Bagno, P., O. Jepsen, and O. Gunnarsson (1989) Ground-state properties of third-row elements with nonlocal density functionals, *Phys. Rev. B*, **40**, 1997-2000.

Baroni, S., S. de Gironcoli, A. Dal Corso, and P. Giannozzi (2001) Phonons and related crystal properties from density-functional perturbation theory, *Rev. Mod. Phys.*, **73**, 515-562.

Boehler, R. (1993) Temperature in the earth's core from melting-point measurements of iron at high static pressures, *Nature*, **363** 534-536.

Born, M., and K. Huang (1954) Dynamical Theory of Crystal Lattices, *Oxford Univ. Press, New York*.

Caracas, R., R. Wentzcovitch, G. D. Price, and J. Brodholt (2005) $CaSiO_3$ Perovskite at lower mantle pressures, *Geophys. Res. Lett.* **32**, 06306.

Ceperley, D., and B. Alder (1980) Ground state of the electron gas by a stochastic method, *Phys. Rev. Lett.*, **45**, 566-569.

Cohen, R.E. (1991) Bonding and elasticity of stishovite at high pressure: Linearized augmented plane wave calculations, *Am. Mineral.*, **76**, 733-742.

Demuth, T., Y. Jeanvoine, J. Hafner, and J.G. Angyan (1999) Polymorphism in silica studied in the local density and generalized-gradient approximations, *J. Phys.: Condens. Matter*, **11**, 3833-3874.

Fiquet, G., A. Dewaele, D. Andrault, M. Kunz, and T. Le Bihan (2000) Thermoelastic properties and crystal structure of MgSiO3 perovskite at lower mantle pressure and temperature conditions, *Geophys. Res. Lett.*, **27**, 21-24.

Hamann, D.R. (1996) Generalized gradient theory for silica phase transitions, *Phys. Rev. Lett.*, **76**, 660-663.

Hamann, D.R. (1997) H2O hydrogen bonding in density-functional theory, *Phys. Rev. B*, **55**, R10157-R10160.

Hamann, D.R., M. Schl¨uter, and C. Chiang (1979) Norm-conserving pseudopotentials, *Phys. Rev. Lett.*, **43**, 1494-1497.

Helffrich, G.R., and B.J. Wood (2001) The Earth's mantle, *Nature*, **412**, 501-507.

Hill, R. (1963) Elastic properties of reinforced solids: Some theoretical principles, *J. Mech. Phys. Solids*, **11**, 357-372.

Hohenberg, P., and W. Kohn (1964) Inhomogeneous electron gas, *Phys. Rev.*, **136**, B864-871.

Hyde, B., and S. Andersson (1989) Inorganic Crystal Structures, *Wiley, New York*.

Ita, J., and S.D. King (1998) The influence of thermodynamic formulation on simulations of subduction zone geometry and history, *Geophys. Res. Lett.*, **25**, 1463-1466.

Iitaka, T., K. Hirose, K. Kawamura, and M. Murakami (2004) The elasticity of the $MgSiO_3$ post-perovsktie phase in the Earth's lowermost mantle, *Nature*, **430**, 442-445.

Karato, S. (1998) Some remarks on the origin of seismic anisotropy in the D" layer, *Earth Planets Space*, **50**, 1019-1028.

Karki, B.B., R.M. Wentzcovitch, S. de Gironcoli, and S. Baroni (1999) First-principles determination of elastic anisotropy and wave velocities of MgO at lower mantle conditions, *Science*, **286**, 1705-1707.

Karki, B.B., R.M. Wentzcovitch, S. de Gironcoli, and S. Baroni (2000a) Ab initio lattice dynamics of $MgSiO_3$ perovskite at high pressure, *Phys. Rev. B*, **62**, 14750-14756.

Karki, B.B., R.M. Wentzcovitch, S. de Gironcoli, and S. Baroni (2000b) High-pressure lattice dynamics and thermoelasticity of MgO, *Phys. Rev. B*, **61**, 8793-8800.

Karki, B.B., R.M. Wentzcovitch, S. de Giuroncoli, and S. Baroni (2001) High-pressure elastic properties of major materials of earth's mantle from first principles, *Geophys. Res. Lett.*, **28**, 2699-2702.

Kendall, J.-M., and P.G. Silver (1996) Constraints from seismic anisotropy on the nature of the lowermost mantle, *Nature*, **381**, 409-412.

Knittle, E., and R. Jeanloz (1987) Synthesis and equation of state of $(Mg,Fe)SiO_3$ perovskite to over 100 gigapascals, *Science*, **235**, 668-670.

Kohn, W., and L.J. Sham (1965) Self-consistent equations including exchange and correlation effects, *Phys. Rev.*, **140**, A1133-A1138.

Lay, T., E.J. Garnero, and Q. Williams (2004) Partial melting in a thermo-chemical boundary layer at the base of mantle, *Phys. Earth Planet. Int.*, **146**, 441-467.

Lay, T., and D.V. Helmberger (1983) A lower mantle S wave triplication and the shear velocity structure of D", *Geophys. J. R. Astron. Soc.*, **75**, 799-838.

Lay, T., Q. Williams, and E.J. Garnero (1998) The core-mantle boundary layer and deep earth dynamics, *Science*, **392**, 461-468.

Liu, L.-G. (1974) Silicate perovskite from phase transformation of pyrope-garnet at high pressure and temperature, *Geophys. Res. lett.*, **1**, 277-280.

Mao, W.L. et al. (2004) Ferromagnesian postperovskite silicates in the D" layer of the Earth, *Proc. Natl. Acad. Sci.*, **101**, 15867-15869.

Maruyama, S. (2005) Talk in *International workshop on the post-perovskite phase transition in the Earth's deep mantle*, Tokyo Inst. Tech.

Masters, G., G. Laske, H. Bolton, A. Dziewonski (2000) The relative behavior of shear velocity, bulk sound speed, and compressional velocity in the mantle: Implications for chemical and thermal structure, in: S. Karato, A. Forte, R. Liebermann, G. Masters, L. Stixrude (Eds.), *Earth's Deep Interior*, Geophysical Monograph. vol. 117, American Geophysical Union, Washington, DC, pp. 63-87.

Matyska, C., and D.A. Yuen (2005) The importance of radiative heat transfer on superplumes in the lower mantle with the new post-perovskite phase change, it Earth Planet. Sci. Lett., **234**, 71-81.

McNamara, A.K., P.E. van Keken, and S. Karato (2002), Development of anisotropic structure in the Earth's lower mantle by solid-state convection, *Nature*, **416**, 310-314.

Meade, C., H.K. Mao, and J. Hu (1995) High-temperature phase transition and dissociation of (Mg,Fe)SiO_3 perovskite at lower mantle pressures, *Science*, **268**, 1743-1745.

Murakami, M. et al. (2004) Post-perovskite phase transition in $MgSiO_3$, *Science*, **304**, 855-858.

Murakami M., K. Hirose, N. Sata, Y. Ohishi (2005) Post-perovskite phase transition and mineral chemistry in the pyrolitic lowermost mantle, *Geophys. Res. Lett.*, **32**, L03304, doi:10.1029/2004GL021956.

Musgrave, M.J.P. (1970) Crystal acoustics, *Holden-Day, Boca Raton, Fla*.

Nakagawa, T., and P.J. Tackley (2004) Effects of a perovskite-post perovskite phase change near core-mantle boundary in compressible mantle convection, *Geophys. Res. Lett.*, **31**, L16611, doi:10.1029/2004GL020648.

Nastar, M., and F. Willaime (1995) Tight-binding calculation of the elastic constants of fcc and hcp transition metals, *Phys. Rev. B*, **51**, 6896-6907.

Nielsen, O.H., and R.M. Martin (1985) Stresses in semiconductors: Ab initio calculations on Si, Ge, and GaAs, *Phys. Rev. B*, **32**, 3792-3805.

Oganov, A.R., and S. Ono (2004) Theoretical and experimental evidence for a postperovskite phase of $MgSiO_3$ in Earth's D" layer, *Nature*, **430**, 445-448.

Ono, S., T. Kikegawa, and Y. Ohishi (2005a) A high-pressure and high-temperature synthesis of platinum carbide, Solid State Comm, **133**, 55-59.

Ono S., Y. Ohishi, M. Isshiki, and T. Watanuki (2005b) In situ X-ray observations of phase assemblages in peridotite and basalt compositions at lower mantle conditions:
Implications for density of subducted oceanic plate, *J. Geophys. Res.*, **110**, B02208, doi:10.1029/2004JB003196.

Perdew, J.P., K. Burke, and M. Ernzerhof (1996) Generalized gradient approximation made simple, *Phys. Rev. Lett.*, **77**, 3865-3868.

Perdew, J., and A. Zunger (1981) Self-interaction correction to density functional approximations for many-electron systems, *Phys. Rev., B*, **23**, 5048-5079.

Pulliam, J., and M.K. Sen (1998) Seismic anisotropy in the core-mantle transition zone, *Geophys. J. Int.*, **135**, 113-128.

Saxena, S.K. et al. (1996) Stability of perovskite ($MgSiO_3$) in the earth's mantle, *Science*, **274**, 1357-1359.

Shim, S.-H., T.S. Duffy, and G. Shen (2001) Stability and structure of $MgSiO_3$ perovskite to 2300-kilometer depth in earth's mantle, *Science*, **293**, 2437-2440.

Sidorin, I., M. Gurnis, and D.V. Helmberger (1999) Evidence for a ubiquitous seismic discontinuity at the base of the mantle, *Science*, **286**, 1326-1331.

Stackhouse, S. et al. (2005) The effect of temperature on the seismic anisotropy of the perovskite and post-perovskite polymorphs of $MgSiO_3$, *Earth Planet. Sci. Lett.*, **230**, 1-10.

Steinle-Neumann, G., L. Stixrude, and R. E. Cohen (1999) First-principles elastic constants for the hcp transition metals Fe, Co, and Re at high pressure, *Phys. Rev. B*, **60**, 791-799.

Stixrude, L., R.E. Cohen, and D.J. Singh (1994) Iron at high pressure: Linearized-augmented-plane-wave computations in the generalized-gradient approximation, *Phys. Rev. B*, **50**, 6442-6445.

Troullier, N., and J.L. Martins (1991) Efficient pseudopotentials for plane-wave calculations, *Phys. Rev. B*, **43**, 1993-2006.

Tsuchiya, J., T. Tsuchiya, and R.M. Wentzcovitch (2005a) Vibrational and thermodynamic properties of $MgSiO_3$ postperovskite, *J. Geophys. Res.*, **110**, B02204, doi:10.1029/2004JB003409.

Tsuchiya, J., T. Tsuchiya, and R.M. Wentzcovitch (2005b) Post-Rh_2O_3(II) transition and the high *P, T* phase diagram of alumina, *Phys. Rev. B*, **72**, 020103(R).

Tsuchiya, T., R. Caracas, and J. Tsuchiya (2004a) First principles determination of the phase boundaries of high-presusre polymorphs of silica, *Geophys. Res. Lett.*, **31**, L11610, doi:10.1029/2004GL019649.

Tsuchiya, T., and K. Kawamura (2001) Systematics of elasticity: Ab initio study in B1-type alkaline earth oxides, *J. Chem. Phys.*, **114**, 10086-10093.

Tsuchiya, T., J. Tsuchiya, K. Umemoto, and R.M.Wentzcovitch (2004b) Phase transition in $MgSiO_3$ perovskite in the Earth's lower mantle, *Earth Planet. Sci. Lett.*, **224**, 241-248.

Tsuchiya, T., J. Tsuchiya, K. Umemoto, and R.M. Wentzcovitch (2004c) Elasticity of post-perovskite $MgSiO_3$, *Geophys. Res. Lett.*, **31**, L14603, doi:10.1029/2004GL020278.

Vanderbilt, D. (1990) Soft self-consistent pseudopotentials in a generalized eigenvalue formalism, *Phys. Rev. B*, **41**, 7892-7895.

Wallace, D. (1972) Thermodynamics of Crystals, *Wiley, New York*.

Wentzcovitch, R.M., B.B. Karki, M. Cococcioni, and S. de Gironcoli (2004a) Thermoelastic properties of $MgSiO_3$ perovskite: insights on the nature of earth's lower mantle, *Phys. Rev. Lett.*, **92**, 018501.

Wentzcovitch, R.M., B.B. Karki, S. Karato, and C.R.S. Da Silva (1998) High pressure elastic anisotropy of $MgSiO_3$ perovskite and geophysical implications, *Earth Planet. Sci. Lett.*, **164**, 371-378.

Wentzcovitch, R.M., J.L. Martins, and G.D. Price (1993) Ab initio molecular dynamics with variable cell shape: Application to MgSiO3, *Phys. Rev. Lett.*, **70**, 3947-3950.

Wentzcovitch, R.M., N. Ross, and G.D. Price (1995) Ab initio study of $MgSiO_3$ and $CaSiO_3$ perovskites at lower-mantle pressures, *Phys. Earth Planet. Inter.*, **90**, 101-112.

Wentzcovitch, R.M., L. Stixrude, B.B. Karki, and B. Kiefer (2004b) Akimotite to perovskite phase transition in $MgSiO_3$, *Geophys. Res. Lett.*, **31**, L10611, doi:10.1029/2004GL019704.

Williams, Q., and R. Jeanloz (1990) Melting relations in the iron-sulfur system at ultrahigh pressures: implications for the thermal state of the earth, *J. Geophys. Res.*, **95**, 19299-19310.

Wysession, M.E. et al. (1998) Implications of the D" discontinuity in: M. Gurnis, M.E. Wysession, E. Knittle, B. Buffett (Eds.), *The Core-Mantle Boundary Region*, Geodynamic Series. vol. 28, American Geophysical Union, Washington, DC, pp. 273-297.

Wysession, M.E. et al. (1999) Lateral variations in compressional/shear velocities at the base of the mantle, *Science*, **284**, 120-124.

Yamazaki, D., and S. Karato (2002) Fabric development in (Mg,Fe)O during large strain, shear deformation: Implications for seismic anisotropy in Earth's lower mantle, *Phys. Earth Planet. Inter.*, **131**, 251-267.